

Supporting Information

**Invoking Ultralong Room Temperature Phosphorescence of Purely Organic Compounds
through H-Aggregation Engineering**

Jie Yuan,¹ Shuang Wang,¹ Yu Ji,¹ Runfeng Chen,^{*1} Qi Zhu,¹ Yongrong Wang,¹ Chao Zheng,¹ Ye Tao,¹ Quli Fan,^{*1} Wei
Huang^{*1}

¹Key Laboratory for Organic Electronics and Information Displays & Jiangsu Key Laboratory for Biosensors, Institute of Advanced Materials (IAM),

Jiangsu National Synergetic Innovation Center for Advanced Materials (SICAM), Nanjing University of Posts & Telecommunications, 9 Wenyuan

Road, Nanjing 210023, China.

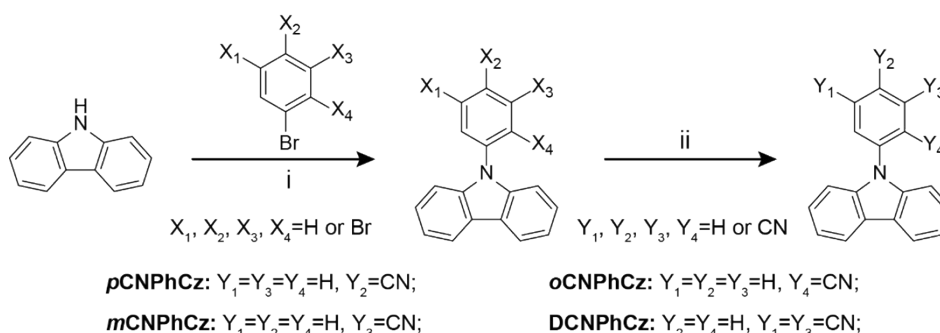
Content

1. Synthesis and characterization	2
2. Single crystal X-ray analysis	4
3. Photophysical property investigation	7
4. Photophysical modeling.....	15
5. Time-dependent density functional theory (TD-DFT) calculation.....	18
6. Bioimaging application	23

1. Synthesis and characterization

Chemicals and solvents purchased from Aldrich or Acros are of analytical grade and were used without further purification. Unless otherwise noted, reactions were carried out under a dry nitrogen atmosphere using standard Schlenk techniques.

^1H and ^{13}C -nuclear magnetic resonance (NMR) spectra were recorded on a Bruker Ultra Shield Plus 400 MHz instrument with CDCl_3 as the solvent and tetramethylsilane (TMS) as the internal standard. Chemical shifts (δ) are given in ppm in Hz. Splitting patterns were designed as follows: s (singlet), d (doublet), and m (multiplet). Mass spectra were obtained using an Agilent GCMS-7890B/5977B instrument. Elemental analyses were performed on an Elementar Vario MICRO elemental analyzer.



Scheme S1. Synthetic route of the organic afterglow molecules of **pCNPhCz**, **mCNPhCz**, **oCNPhCz** and **DCNPhCz**: (i) nitrobenzene, 180°C , 24 h; (ii) coppercyanide, N,N-Dimethylformamide, 180°C , 48 h.

9-(4-Bromophenyl)-9H-carbazole (pBrPhCz): To a 250 mL round bottom flask charged with a stir bar was added 9H-carbazole (3.34 g, 20 mmol), copper (0.56 g, 8.8 mmol), potassium carbonate (11.17 g, 80.8 mmol), 1,4-dibromobenzene (7.00 g, 30 mmol), and 50 mL dry nitrobenzene. The mixture under nitrogen protection was reacted at 180°C for 24 h¹. After cooling to room temperature, the solvent of nitrobenzene was removed by vacuum distillation. The resulting solid was dissolved in 120 mL dichloromethane (DCM) and washed with brine (60 mL). The mixture was then extracted with DCM for three times. The organic phase was collected and dried over MgSO_4 . After removing the solvent under reduced pressure, the crude product was purified by column chromatograph (using petroleum ether: DCM = 10:1 as the eluent) to obtain a

colorless powder. Yield: 7.70 g (80%). ^1H NMR (400 MHz, CDCl_3): δ = 8.16-8.14 (d, 2H), 7.75-7.73 (d, 2H), 7.47-7.37 (m, 6H), 7.33-7.29 (m, 6H). ^{13}C NMR (100 MHz, CDCl_3): δ = 140.61, 136.81, 133.13, 128.74, 126.11, 123.49, 120.91, 120.42, 120.23, 109.56.

9-(3-Bromophenyl)-9H-carbazole (*m*BrPhCz): Similar to the preparation of *p*BrPhCz, *m*BrPhCz was synthesized by using 4.8 mL *m*-dibromobenzene (9.40 g; 40 mmol). Yield: 4.60 g of colorless crystal (72%). ^1H NMR (400 MHz, CDCl_3): δ = 8.30-8.28 (d, 2H), 7.90 (s, 1H), 7.71-7.69 (d, 1H), 7.61-7.44 (m, 8H). ^{13}C NMR (100 MHz, CDCl_3): δ = 140.58, 139.15, 131.15, 130.55, 130.18, 126.16, 125.76, 123.56, 123.25, 120.43, 120.37, 109.65.

9-(2-Bromophenyl)-9H-carbazole (*o*BrPhCz): Similar operation, *o*BrPhCz was prepared from 1-bromo-2-iodobenzene (8.50 g; 30 mmol). Yield: 5.70 g of colorless crystal (90%). ^1H NMR (400 MHz, CDCl_3): δ = 8.18 (d, 2H), 7.88 (d, 1H), 7.54 (m, 2H), 7.46-7.40 (m, 3H), 7.32 (t, 2H), 7.10-7.04 (m, 2H). ^{13}C NMR (101 MHz, CDCl_3): δ = 140.86, 136.76, 134.27, 131.17, 130.20, 128.86, 125.97, 123.88, 123.26, 120.39, 120.02, 110.06.

9-(3,5-Dibromophenyl)-9H-carbazole (DBrPhCz): Similarly, DBrPhCz was prepared from 1,3,5-tribromobenzene (15.96 g; 40 mmol). Yield: 5.10 g of colorless crystal (64%). ^1H NMR (400 MHz, CDCl_3): δ = 8.14-8.12 (d, 2H), 7.77 (t, 1H), 7.71 (d, 2H), 7.70-7.41 (m, 4H), 7.3-7.30 (m, 2H). ^{13}C NMR (100 MHz, CDCl_3): δ = 140.82, 140.23, 140.09, 132.99, 128.83, 126.34, 123.75, 120.77, 120.50, 109.52.

4-(9H-carbazol-9-yl)benzotrile (*p*CNPhCz): To a 250 mL round bottom flask charged with a stir bar was added *p*BrPhCz (3.21 g, 10 mmol), coppercyanide (4.50 g, 50 mmol) and 50 mL dry N,N-dimethylformamide. The mixture under nitrogen protection was reacted at 180°C for 48 hours². After cooling to room temperature, the solvent of N,N-dimethylformamide was removed by vacuum distillation. The resulting solid was dissolved in DCM and washed with brine. The mixture was then extracted with DCM for three times. The organic phase was collected and dried over MgSO_4 . After removing the solvent, the crude product was purified by column chromatograph (using pure petroleum ether as the eluent) and recrystallized from DCM/hexane for several times to obtain a colorless crystal. Yield: 1.80 g (70%). ^1H NMR (400 MHz, CDCl_3): δ = 8.16-8.12 (d, 2H), 7.92-7.90 (d, 2H), 7.75-7.73 (d, 2H), 7.48-7.43 (m, 4H), 7.37-7.26 (m, 2H). ^{13}C NMR (100 MHz, CDCl_3): δ = 142.10, 139.92, 133.94, 127.13, 126.40, 124.03, 121.02, 120.61, 118.39, 110.50, 109.55.

GC-MS (CH₂Cl₂) *m/z*: calculated for C₁₈H₁₃N: 268.1; Found: 268.2. Anal. calcd. for C₁₉H₁₂N₂: C 85.05, H 4.51, N 10.44; found: C 85.32, H 4.27, N 10.44.

3-(9H-carbazol-9-yl)benzotrile (mCNPhCz): Similar to the preparation of *p*CNPhCz, *m*CNPhCz was synthesized by using *m*BrPhCz (3.21 g, 10 mmol). Yield: 1.90 g of colorless crystal (74%). ¹H NMR (400 MHz, CDCl₃): δ= 8.16-8.14 (d, 2H), 7.91-7.85 (m, 2H), 7.77-7.72 (m, 2H), 7.47-7.43 (m, 2H), 7.40-7.32 (m, 4H). ¹³C NMR (100 MHz, CDCl₃): δ= 140.25, 138.93, 131.55, 131.03, 130.78, 130.36, 126.37, 123.77, 120.82, 120.61, 117.97, 114.24, 109.31. GC-MS (CH₂Cl₂) *m/z*: calculated for C₁₈H₁₃N: 268.1; Found: 268.2. Anal. calcd. for C₁₉H₁₂N₂: C 85.05, H 4.51, N 10.44; found: C 85.38, H 4.59, N 10.47.

2-(9H-carbazol-9-yl)benzotrile (oCNPhCz): Similar to the preparation of *p*CNPhCz, *o*CNPhCz was synthesized by using *o*BrPhCz (3.21 g, 10 mmol). Yield: 1.70 g of colorless crystal (65%). ¹H NMR (400 MHz, CDCl₃): δ= 8.16-8.15 (d, 2H), 7.97-7.95 (d, 1H), 7.85-7.81 (m, 1H), 7.64-7.62 (m, 2H), 7.46-7.42 (m, 2H), 7.35-7.32 (m, 2H), 7.26-7.20 (m, 2H). ¹³C NMR (100 MHz, CDCl₃): δ= 140.71, 140.61, 134.59, 134.38, 129.71, 128.52, 126.25, 123.90, 120.83, 120.60, 116.13, 112.82, 109.73. GC-MS (CH₂Cl₂) *m/z*: calculated for C₁₈H₁₃N: 268.1; Found: 268.2. Anal. calcd. for C₁₉H₁₂N₂: C 85.05, H 4.51, N 10.44; found: C 85.04, H 4.41, N 10.22.

5-(9H-carbazol-9-yl)isophthalonitrile (DCNPhCz): Similar to the preparation of *p*CNPhCz, *DCN*PhCz was synthesized by using *DBr*PhCz (2.00 g, 5 mmol). Yield: 0.70 g of colorless crystal (48%). ¹H NMR (400 MHz, CDCl₃): δ= 8.48-8.48 (d, 2H), 7.74-7.66 (m, 4H), 7.62-7.59 (m, 1H), 7.52-7.50 (d, 2H), 7.45-7.43 (d, 2H). ¹³C NMR (100 MHz, CDCl₃): δ= 140.43, 139.57, 133.86, 133.02, 126.82, 124.24, 121.80, 120.91, 116.00, 115.98, 108.88. GC-MS (CH₂Cl₂) *m/z*: calculated for C₁₈H₁₃N: 293.1; Found: 293.2. Anal. calcd. for C₂₀H₁₁N₃: C 81.89, H 3.78, N 14.33; found: C 81.60, H 3.49, N 14.37.

2. Single crystal X-ray analysis

Single crystals were grown from a mixture of DCM and hexane. X-ray diffraction data of these single crystals were collected on a Bruker Smart Apex CCD area detector diffractometer using graphite-monochromated Mo-K α radiation ($\lambda = 0.71073 \text{ \AA}$) at room-temperature or 100 K. A narrow-frame method with scan widths of 0.30° in angular velocity (ω) was applied during the data

collection. Cell parameters were retrieved using SMART software and refined using SAINT on all observed reflections. Structures were solved by direct methods using the SHELX-97 program package. Non-hydrogen atoms were found using alternating difference Fourier syntheses and least-squared refinement cycles and, during the final cycles, were refined anisotropically. Hydrogen atoms were placed in calculated positions and refined as riding atoms with a uniform value of U_{iso}^3 .

Interestingly, the compound of *m*CNPhCz was observed to exhibit two different single crystal structures, which were indentified as *m*CNPhCz and *m*CNPhCz' respectively. Crystallographic parameters of *p*CNPhCz, *m*CNPhCz, *m*CNPhCz', *o*CNPhCz and DCNPhCz were summarized in **Table S1**. CCDC reference numbers for *p*CNPhCz, *m*CNPhCz, *m*CNPhCz', *o*CNPhCz and DCNPhCz are Nos. 135494, 1588870, 1814229, 1581453 and 1581448, respectively.

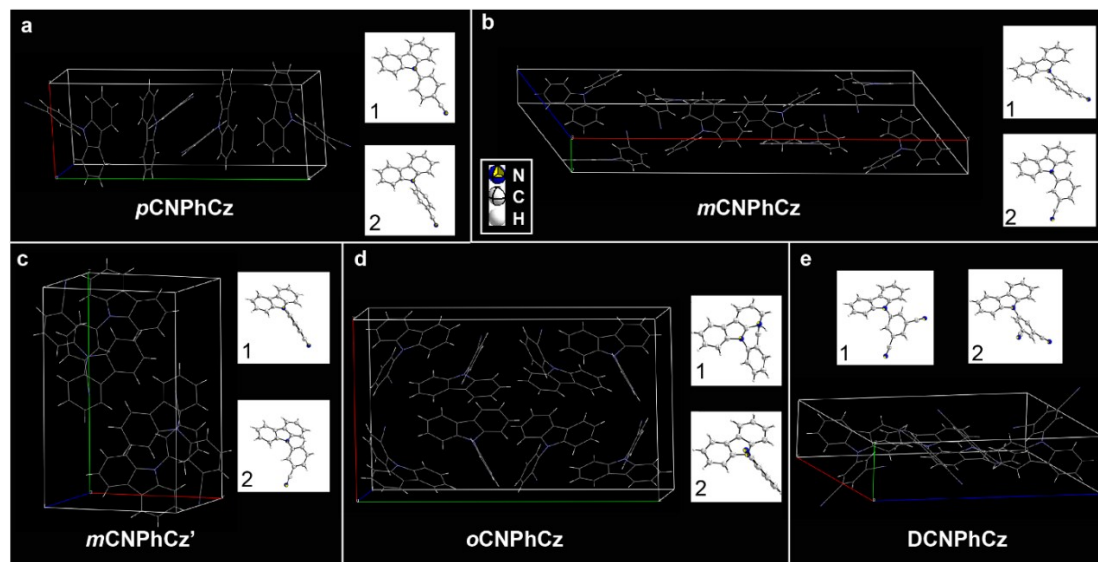


Figure S1. Single-crystal structures of (a) *p*CNPhCz, (b) *m*CNPhCz, (c) *m*CNPhCz', (d) *o*CNPhCz and (e) DCNPhCz. Inserts show the two different conformations of each molecule in crystal.

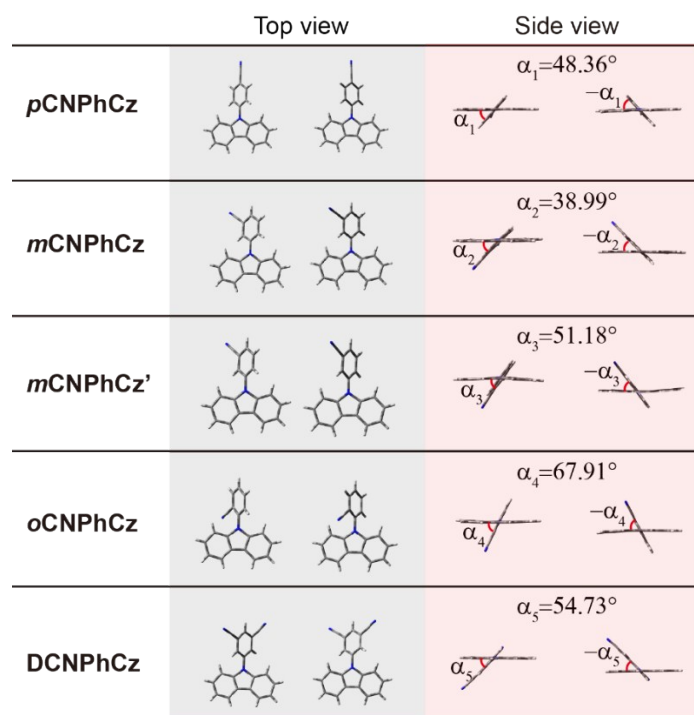


Figure S2. Top-view and side-view of the two different conformations in **pCNPhCz**, **mCNPhCz**, **mCNPhCz'**, **oCNPhCz** and **DCNPhCz** crystals.

Table S1. Structure data of **pCNPhCz**, **mCNPhCz**, **mCNPhCz'**, **oCNPhCz** and **DCNPhCz** single crystals.

Compound	pCNPhCz ⁴	mCNPhCz	mCNPhCz'	oCNPhCz	DCNPhCz
Empirical formula	C ₁₉ H ₁₂ N ₂	C ₂₀ H ₁₁ N ₃			
Ambient temperature (K)	293(2)	100	100	295	295
Formula weight (g mol ⁻¹)	268.31	268.31	268.31	268.31	293.32
Crystal color	colorless	colorless	colorless	colorless	colorless
Wavelength (Å)	0.71073	0.71073	0.71073	0.71073	0.71073
Space Group	P 21/c	C 2/c	P 21/c	Iba2	P21/c
<i>a</i> (Å)	8.2739(12)	41.374(7)	10.231(3)	14.753(3)	16.718(4)
<i>b</i> (Å)	20.681(4)	3.9588(7)	16.032(4)	24.611(4)	4.7260(10)
<i>c</i> (Å)	8.5913(11)	17.309(3)	8.461(2)	8.0508(13)	19.164(4)
α (deg)	90	90	90	90	90
β (deg)	104.937(12)	111.876(4)	93.900(6)	90	95.969(7)
γ (deg)	90	90	90	90	90
<i>V</i> (Å ³)	1420.4(4)	2630.9(8)	1384.6(6)	2923.1(8)	1505.9(6)
<i>Z</i>	4	8	4	8	4
Density (g cm ⁻³)	1.255	1.355	1.278	1.291	1.294
μ (mm ⁻¹)	0.075	0.081	0.077	0.073	0.079
<i>T</i> _{min} , <i>T</i> _{max}	0.937, 0.947	0.855, 0.924	0.912, 0.926	0.594, 0.868	0.981, 0.988
<i>F</i> (000)	560.0	1120.0	560.0	1120.0	608.0
<i>h</i> _{max} , <i>k</i> _{max} , <i>l</i> _{max}	10, 26, 11	66, 6, 22	17, 26, 14	23, 41, 12	22, 6, 25
<i>Theta</i> _{max}	27.480	35.536	36.274	37.616	28.346

3. Photophysical property investigation

Ultraviolet-visible (UV-Vis) spectra were measured using a SHIMADZU UV-3600 UV-VIS-NIR spectrophotometer. Steady-state photoluminescence, phosphorescence spectra, time-resolved excitation spectra, kinetic measurement and quantum yields were performed on an Edinburgh FLS920 fluorescence spectrophotometer. For steady-state photoluminescence, time-resolved excitation spectra and quantum yields measurements, a xenon arc lamp (Xe900) was used; Xe900 can provide excellent steady state excitation source. For phosphorescence spectra, a microsecond flash-lamp (uF900) were used; the uF900 flash lamp produces short, typically a few μs , and high irradiance optical pulses for phosphorescence measurements in the range from microseconds to seconds. The LED flash lamp provides subnanosecond optical pulses over the UV-to-vis spectral range for fluorescence decay measurements. The microsecond flash lamp produces short, typically a few microsecond (μs), and high irradiance optical pulses for the organic ultralong room temperature phosphorescence (OURTP) decay measurements. The lifetimes (τ) of the luminescence were obtained by fitting the decay curve with a multi-exponential decay function⁵ of

$$I(t) = \sum_i A_i e^{-\frac{t}{\tau_i}} \quad (\text{S1})$$

where A_i and τ_i represent the amplitudes and lifetimes of the individual components for multi-exponential decay profiles, respectively. The photographs were recorded by a Nikon D90 camera.

The OURTP yields were generally obtained by peak-differentiation-imitating analysis from the steady-state PL spectrum and the absolute total quantum yield (Φ). By peak-differentiation-imitating analysis, the OURTP ratio can be identified, and from Φ , both fluorescent and OURTP yields can be figured out (Table S3). As illustrated in Equation S2, Φ is obtained by photon counting from the excitation source into an integration sphere with the ratio of photons emitted:

$$\Phi = \frac{N^{em}}{N^{abs}} \quad (\text{S2})$$

In this equation, N^{em} is the number of emitted photons and N^{abs} is the number of absorbed photons.

One of the most important, and experimentally elusive, parameters of intramolecular energy transfer is the rate constant for intersystem crossing from the lowest excited singlet to triplet state, k_{ISC} . Experimentally, k_{ISC} can be estimated as follows⁶:

$$\frac{\Phi^{Ph}}{\tau^F} \leq k_{ISC} \leq \frac{1 - \Phi^F}{\tau^F} \quad (S3)$$

$$k_{ISC}^{min} = \frac{\Phi^{Ph}}{\tau^F} \quad (S4)$$

$$k_{ISC}^{max} = \frac{1 - \Phi^F}{\tau^F} \quad (S5)$$

where Φ^F and Φ^{Ph} represent the photoluminescence quantum yields (PLQY) of fluorescence and phosphorescence, respectively; τ^F represents the lifetime of fluorescence; while k_{ISC}^{min} and k_{ISC}^{max} are the bottom and upper limits of k_{ISC} , respectively.

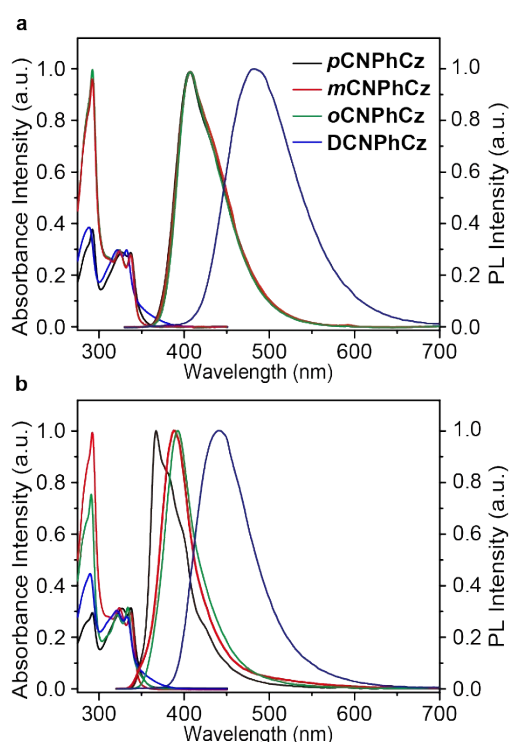


Figure S3. UV-vis absorption and steady-state PL spectra of **pCNPhCz**, **mCNPhCz**, **oCNPhCz** and **DCNPhCz** in (a) dilute CH₂Cl₂ solutions and (b) thin films at room temperature.

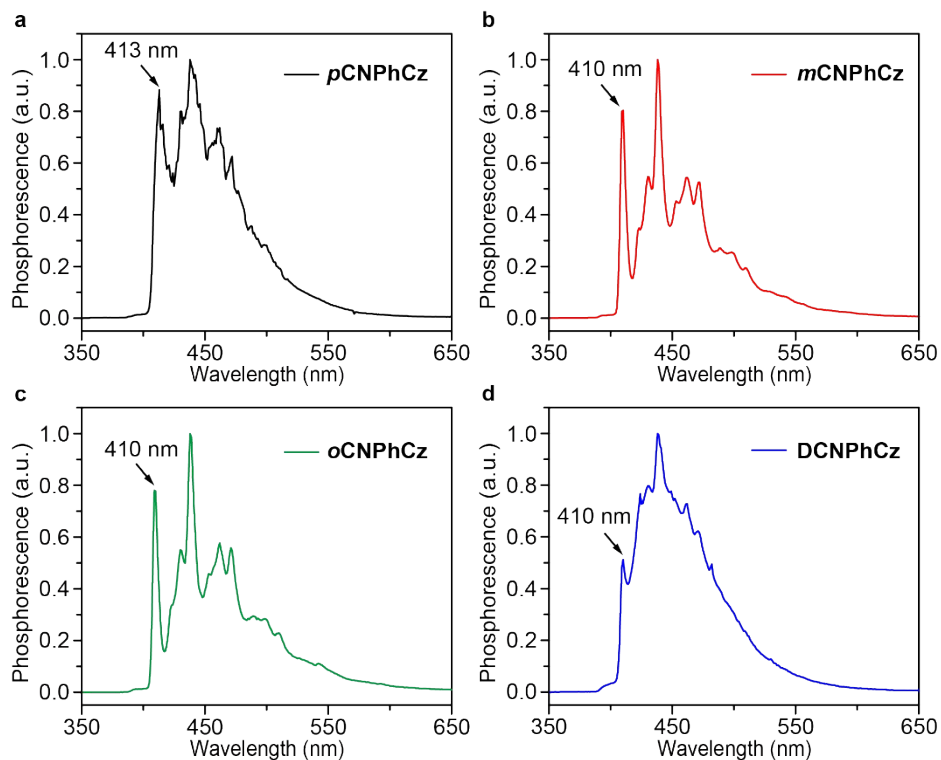


Figure S4. Phosphorescence spectra of (a) *p*CNPhCz, (b) *m*CNPhCz, (c) *o*CNPhCz and (d) DCNPhCz excited at 295 nm in 2-methyltetrahydrofuran at 77 K with a delay time of 10 ms.

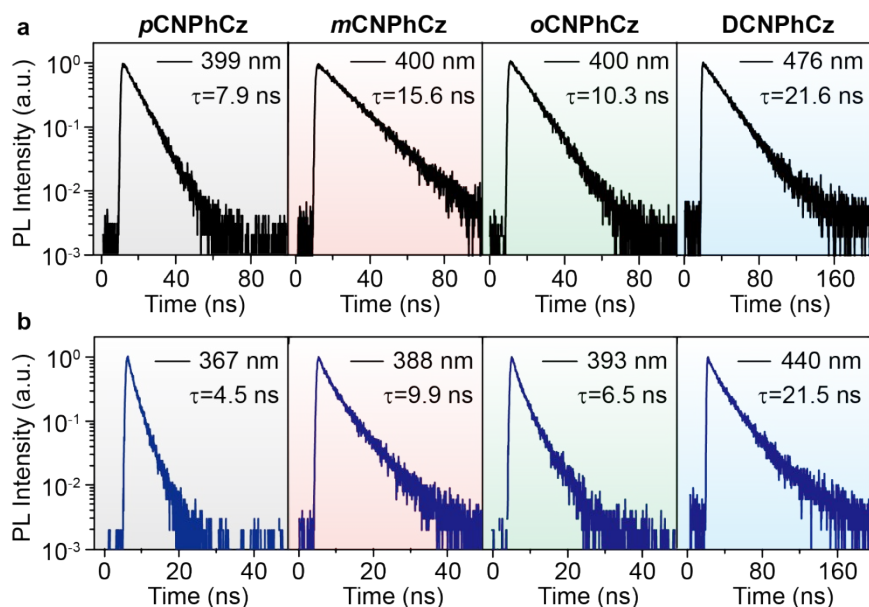


Figure S5. Fluorescence decay curves of *p*CNPhCz, *m*CNPhCz, *o*CNPhCz and DCNPhCz in (a) dilute CH₂Cl₂ solutions and (b) thin films excited by 290 nm irradiation at room temperature.

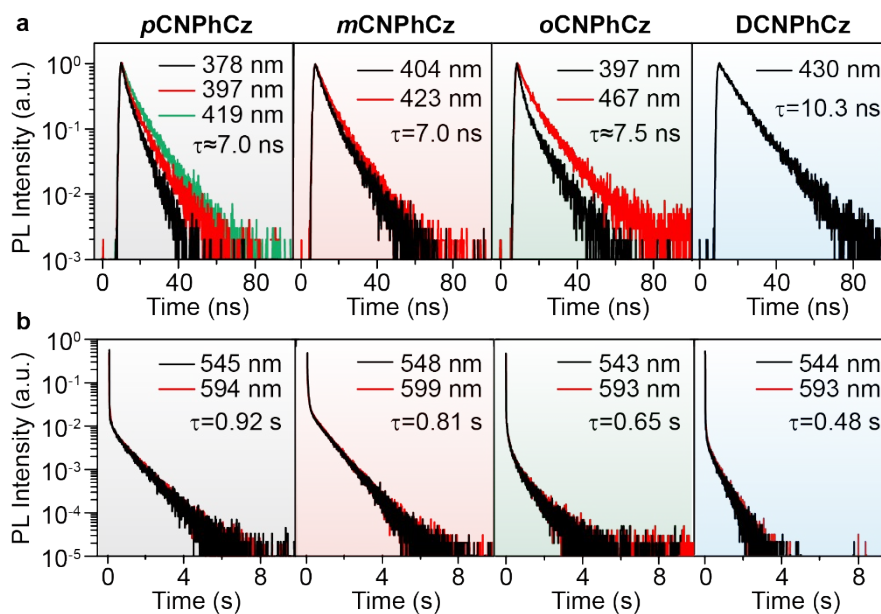


Figure S6. (a) Fluorescence (excited at 290 nm) and (b) OURTP (excited at 365 nm) decay curves of *p*CNPhCz, *m*CNPhCz, *o*CNPhCz and DCNPhCz crystals at room temperature.

Table S2. Photoluminescence properties and kinetic parameters of OURTP molecules in dilute CH₂Cl₂ solution.

Compound	Fluorescence ^a			Phosphorescence ^b		ISC	
	λ (nm)	τ ^F (ns)	Φ ^F (%)	λ (nm)	Φ ^{Ph} (%)	k _{min} ISC (s ⁻¹)	k _{max} ISC (s ⁻¹)
PhCz	349/364	5.5	75.8	410	4.8	8.7×10 ⁶	4.4×10 ⁷
<i>p</i> CNPhCz	399	5.6	44.5	413	6.7	1.2×10 ⁷	7.0×10 ⁷
<i>m</i> CNPhCz	400	5.5	20.0	410	18.6	3.4×10 ⁷	5.1×10 ⁷
<i>o</i> CNPhCz	400	5.6	19.7	410	17.6	3.1×10 ⁷	7.8×10 ⁷
DCNPhCz	476	19.0	11.2	410	19.4	1.0×10 ⁷	4.1×10 ⁷

^a: at room temperature; ^b: at 77 K.

Table S3. Absolute quantum efficiency measurements of OURTP crystals.

Compound	Φ (%)	OURTP ratio	Φ ^F (%)	Φ ^{Ph} (%)
<i>p</i> CNPhCz	34.3	0.06	32.5	1.8
<i>m</i> CNPhCz	24.2	0.18	20.5	3.7
<i>o</i> CNPhCz	20.0	0.17	17.1	2.9
DCNPhCz	39.5	0.27	31.9	8.6

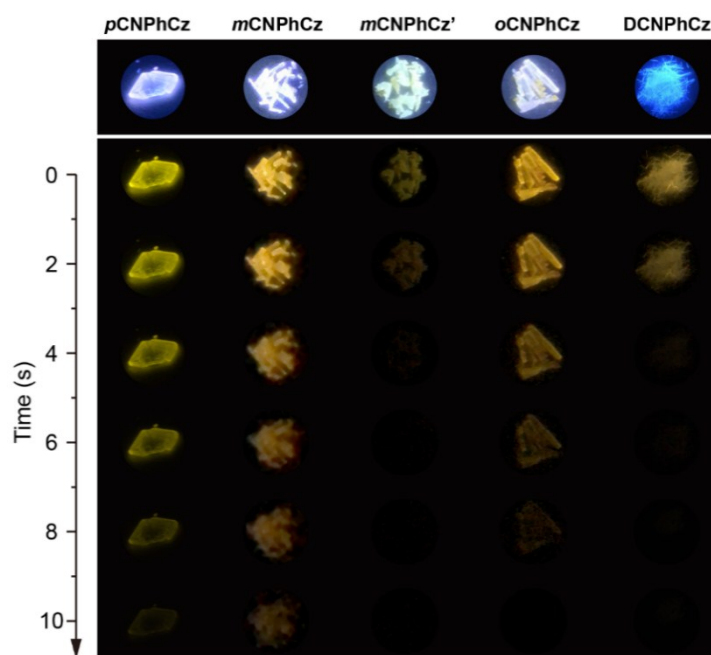


Figure S7. Photographs of *pCNPhCz*, *mCNPhCz*, *mCNPhCz'*, *oCNPhCz* and *DCNPhCz* crystals taken at different time intervals before (first row) and after (succeeding rows) turn-off of the photoexcitation (365 nm) under ambient conditions.

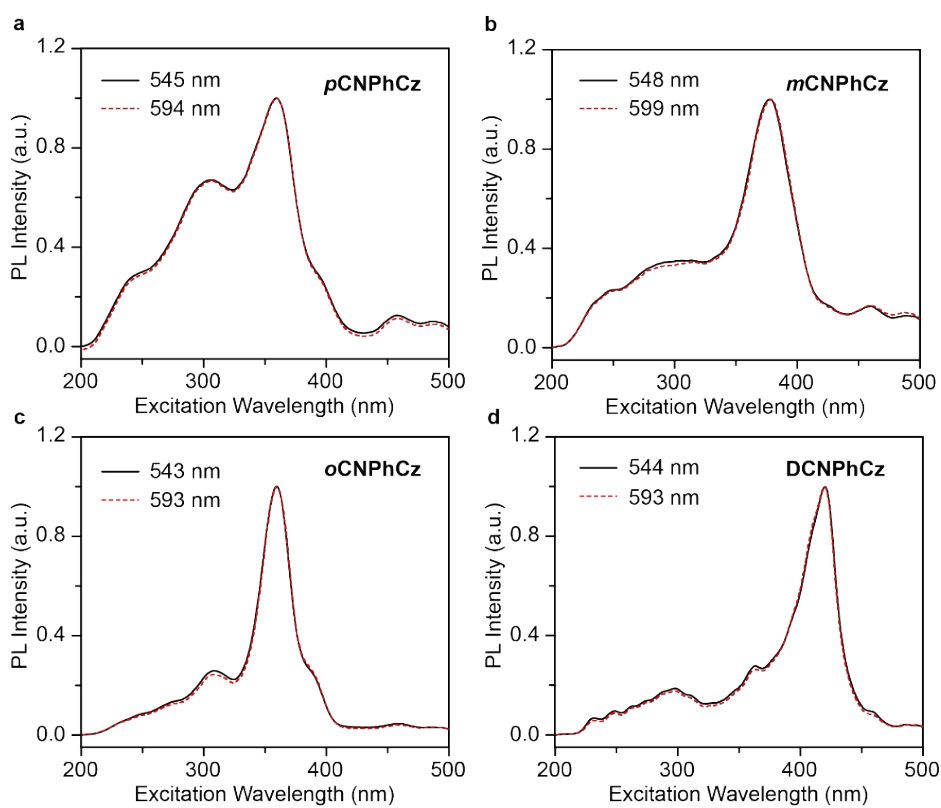


Figure S8. Excitation spectra of OURTP peaks of (a) *pCNPhCz* (545, 594 nm), (b) *mCNPhCz* (548, 599 nm), (c) *oCNPhCz* (543, 590 nm) and (d) *DCNPhCz* (548, 597 nm) crystals at room-temperature.

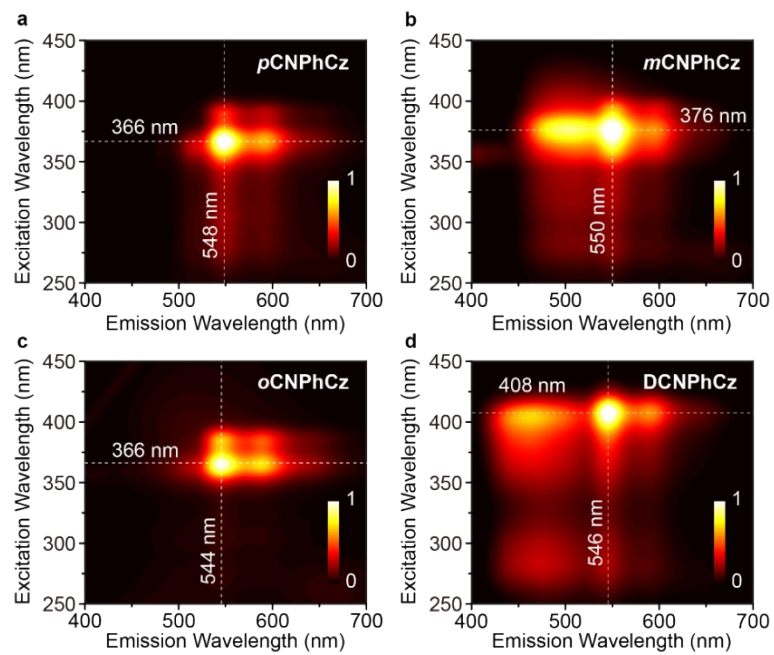


Figure S9. Excitation-phosphorescence mapping of (a) *p*CNPhCz, (b) *m*CNPhCz, (c) *o*CNPhCz and (d) DCNPhCz crystals at room temperature with 5 ms delay.

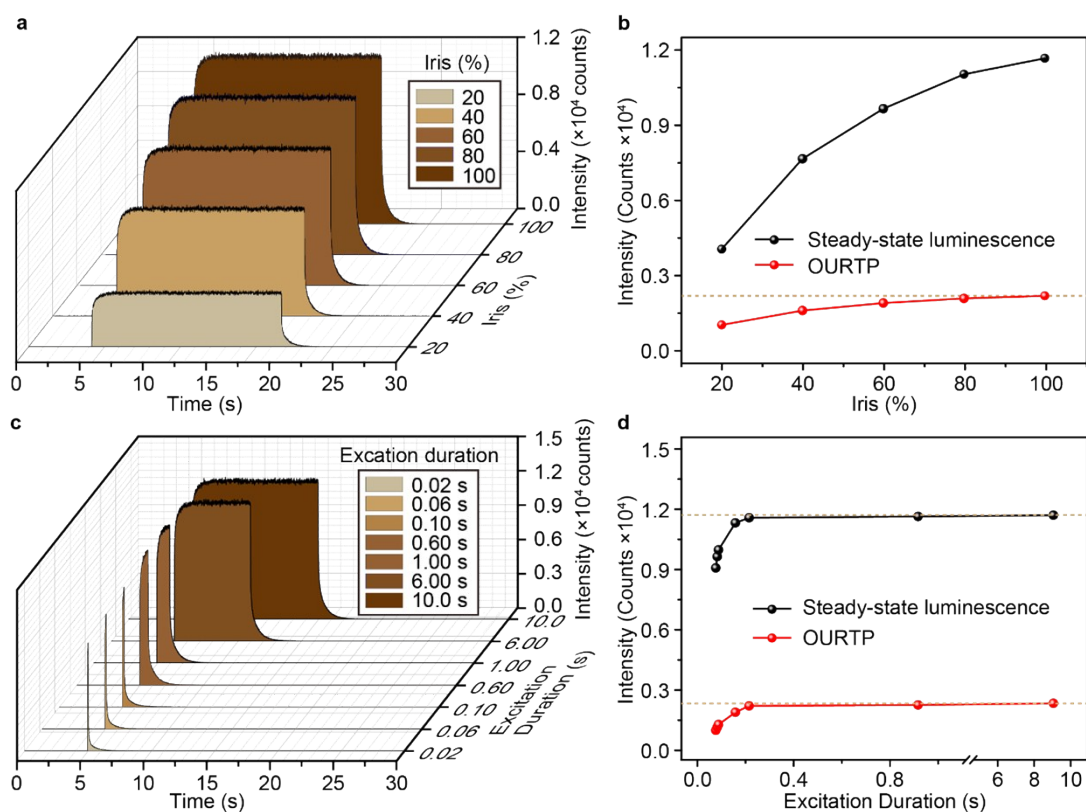


Figure S10. The influence of excitation strength (a, b) and excitation duration (c, d) on OURTP emission (548 nm) of *m*CNPhCz crystal under ambient conditions. Intensity profile of the 548 nm emission (a) as a function of time and different Iris (20, 40, 60, 80 and 100 %) and the strength of the steady-state and afterglow OURTP emission (b) excited at 378 nm at room temperature. The sample was irradiated for 10 s, during which time the steady state luminescence (548 nm) strength was measured. The OURTP intensity was measured by collecting all the afterglow emission photons when the excitation source was switched off. Intensity profiles of the 548 nm emission as a function of time (c) and the corresponding intensities of the steady-state and afterglow OURTP emission (d) upon excitation of 378 nm light with different irradiating time under ambient conditions. The sample was irradiated for 0.02, 0.06, 0.1, 0.6, 1.0, 6.0 and 10 s, respectively.

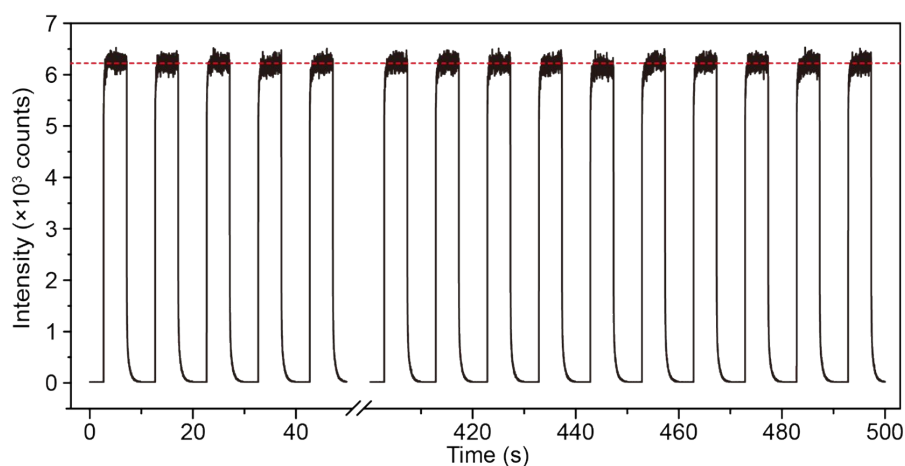


Figure S11. Time-dependent PL (548 nm) intensity scan of *m*CNPhCz crystal under ambient conditions for 50 times with the excitation (378 nm) switched on and off for 2.5 and 5 s, respectively.

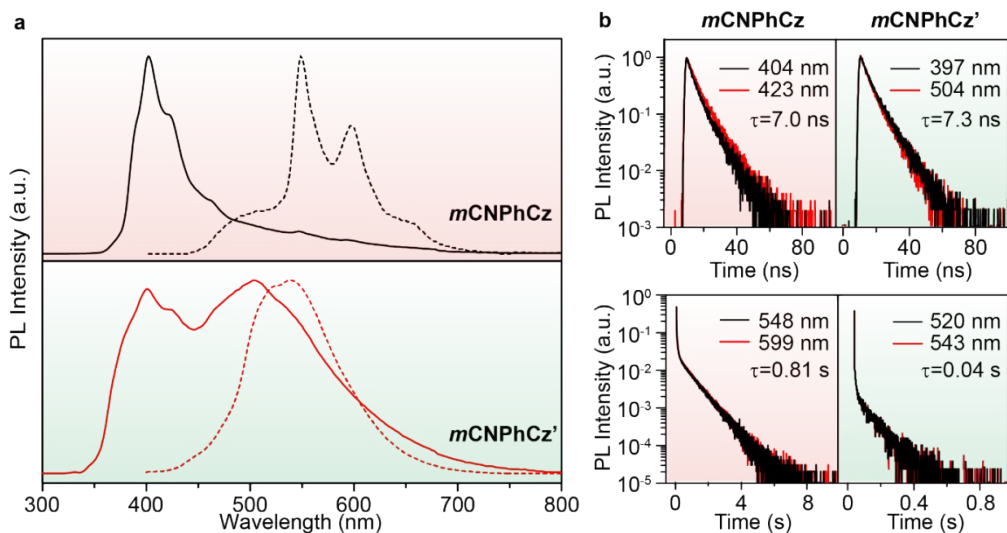


Figure S12. (a) Steady-state photoluminescent (PL) spectra (in solid line) and OURTP spectra (in dashed line) of *mCNPhCz* and *mCNPhCz'* crystals and their (b) fluorescence and OURTP decay curves excited by 295 nm irradiation at room temperature. A delay time of 10 ms was applied to obtain the OURTP spectra.

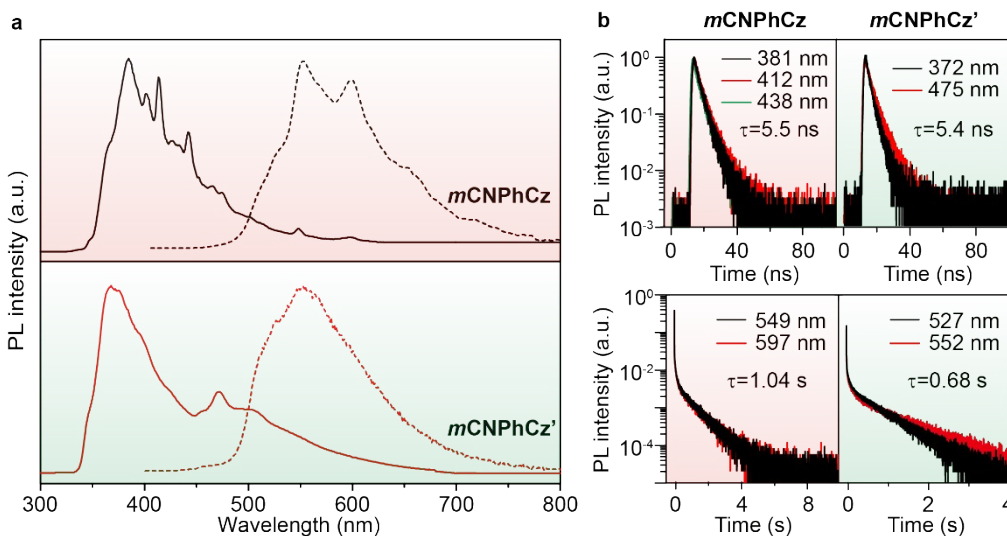


Figure S13. (a) Steady-state photoluminescent (PL) spectra (in solid line) and OURTP spectra (in dashed line) of *mCNPhCz* and *mCNPhCz'* crystals and their (b) fluorescence and OURTP decay curves excited by 295 nm irradiation at 77 K. A delay time of 10 ms was applied to obtain the OURTP spectra.

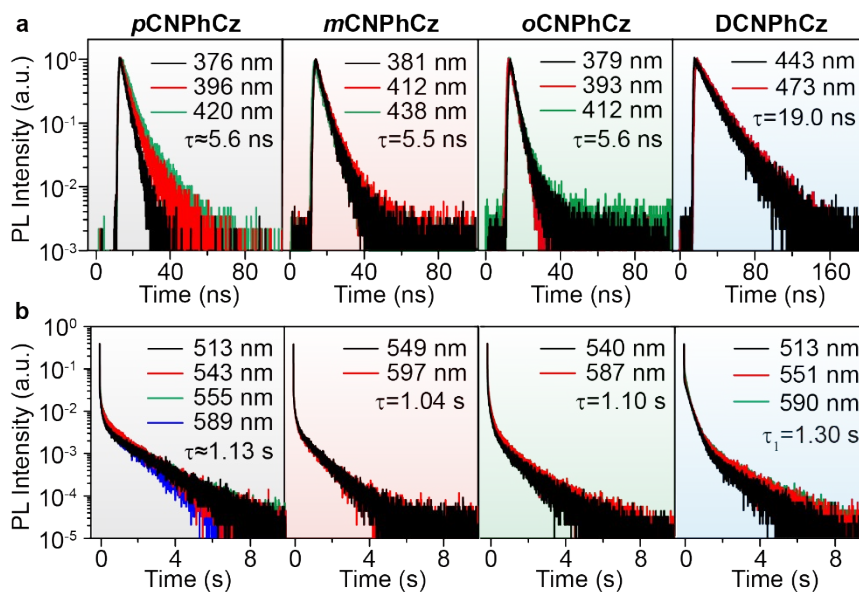
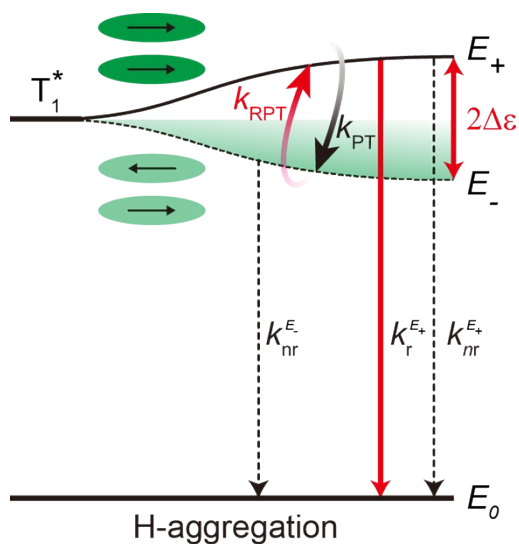


Figure S14. (a) Fluorescence (excited at 290 nm) and (b) OURTP (excited at 365 nm) decay curves of *p*CNPhCz, *m*CNPhCz, *o*CNPhCz and DCNPhCz crystals at 77 K.

4. Photophysical modeling



Scheme S2. Photophysical decay processes for the OURTP of H-aggregates. Note that $k_{r}^{E_+}$ and $k_{nr}^{E_+}$ are the radiative and non-radiative decay rate constants of E_+ , respectively, $k_{nr}^{E_-}$ is the non-radiative decay rate constants of E_- ; k_{PT} and k_{RPT} are the phase transformation (PT) and reverse PT rate constants, respectively.

According to Frenkel exciton theory⁷, the Coulomb coupling between molecules in aggregates leads to the formation of two delocalized excited states (the in- and out-of-phase states) split by $2|\Delta\epsilon|$, where $\Delta\epsilon$ is exciton splitting energy. The in-phase state, shifted by $\Delta\epsilon$, is characterized by

an enhanced transition dipole moment relative to the monomer, whereas the out-of-phase state, shifted by $\Delta\varepsilon$, is optically dark due to a cancellation of the transition dipole moments. The $\Delta\varepsilon$ in the case of dimer is given by:

$$\Delta\varepsilon = \frac{2|M|^2}{r_{uv}^3} (\cos \alpha - 3 \cos \theta_1 \cos \theta_2) \quad (S6)$$

where M is the electric dipole transition moment, α is the angle between the transition moments of the two molecules in the dimer, and θ_1 and θ_2 are the angles between transition moments of the two molecules and the interconnection of the centers respectively, r_{uv} is the distance between the point dipoles in molecules u and v . As a result, when $\Delta\varepsilon > 0$, it belongs to H-aggregation, and when $\Delta\varepsilon < 0$, it is J-aggregation.

In H-aggregates with $\Delta\varepsilon > 0$, there is rapid intraband relaxation subsequent to photoabsorption, leading to efficient population of the lowest energy state; because this state is characterized by the out-of-phase alignment of transition dipoles, it has no direct radiative coupling to the ground state for emission, which is forbidden by symmetry. However, with the aid of symmetry-breaking disorder or vibronic coupling, emission of H-aggregates is also possible by the reverse phase transformation (RPT) from the low-lying non-emissive out-of-phase state (E_-) to the high-lying emissive in-phase state (E_+).

Theoretically, the concentration decay of E_+ and E_- after the removal of the UV-excitation can be described in Equations S7-8 under consideration of their all decay channels as illustrated in Figure S15.

$$\frac{d[E_+]}{d[t]} = k_{RPT} [E_-] - (k_r^{E_+} + k_{nr}^{E_+} + k_{PT}) [E_+] \quad (S7)$$

$$\frac{d[E_-]}{d[t]} = -(k_{RPT} + k_{nr}^{E_-}) [E_-] + k_{PT} [E_+] \quad (S8)$$

where $k_r^{E_+}$ and $k_{nr}^{E_+}$ are the radiative and non-radiative decay rate constants of E_+ respectively; $k_{nr}^{E_-}$ is the non-radiative decay rate constants of E_- ; k_{PT} and k_{RPT} are the PT and RPT rate constants, respectively. The solutions of these differential equations are in biexponential forms

$$[E_+] = C_1 \exp(-k_P^{E_+} t) + C_2 \exp(-k_D^{E_+} t) \quad (S9)$$

where , $kE_+ P$ and $kE_+ D$ are the prompt and delayed rate constants of E_+ , respectively; they can be illustrated in following formulas:

$$k_p^{E_+}, k_D^{E_+} = \frac{k_r^{E_+} + k_{nr}^{E_+} + k_{PT} + k_{RPT}}{2} \times \left(1 \pm \sqrt{1 - \frac{4(k_r^{E_+} + k_{nr}^{E_+} + k_{PT})(k_{nr}^{E_+} + k_{RPT}) - 4k_{PT}k_{RPT}}{(k_r^{E_+} + k_{nr}^{E_+} + k_{PT} + k_{nr}^{E_+} + k_{RPT})^2}} \right) \quad (S10)$$

Since there are negligible deactivation channels from E_+ , the values of $kE_+ r$, $kE_+ nr$ and k_{PT} are significantly larger than those of $kE_+ nr$ and k_{RPT} . As a result, $kE_+ P$ and $kE_+ D$ can be approximated by the following formulas:

$$k_p^{E_+} = k_r^{E_+} + k_{nr}^{E_+} + k_{PT} \quad (S11)$$

$$k_D^{E_+} = k_{nr}^{E_+} + \left(1 - \frac{k_{PT}}{k_r^{E_+} + k_{nr}^{E_+} + k_{PT}}\right) k_{RPT} \quad (S12)$$

Considering that $kE_+ r$ and $kE_+ nr$ are much larger than k_{PT} , $kE_+ P$ and $kE_+ D$ can be further approximated:

$$k_p^{E_+} = k_r^{E_+} + k_{nr}^{E_+} \quad (S13)$$

$$k_D^{E_+} = k_{nr}^{E_+} + k_{RPT} \quad (S14)$$

For luminescent H-aggregates, $kE_+ nr$ is very small ($\ll k_{RPT}$). Therefore,

$$k_D^{E_+} = k_{RPT} \quad (S15)$$

Thus, the $\tau E_+ P$ and $\tau E_+ D$ can be deduced as in Equation S16-17:

$$\tau_P^{E_+} = \frac{\Phi_P}{k_p^{E_+}} = \frac{\Phi_P}{k_r^{E_+} + k_{nr}^{E_+}} \quad (S16)$$

$$\tau_D^{E_+} = \frac{\Phi_D}{k_D^{E_+}} = \frac{\Phi_{T^*} - \Phi_P}{k_{RPT}} \quad (S17)$$

where Φ_{T^*} is the quantum efficiency of the OURTP emission, and Φ_P and Φ_D are the quantum efficiency of the prompt and delayed component of the OURTP emission, respectively.

For aggregates with N -coupled chromophores, the delocalized excited states are generally described as molecular excitons, which abide by the Frenkel exciton Hamiltonian

$$H_{ex} = E_M + D + \sum_{m,n} J_{m,n} |m\rangle\langle n| \quad (S18)$$

where E_M is the monomer transition energy and D is the gas-to-crystal frequency shift, reflecting the ability of neighboring molecules to better stabilize an excited state *via* non-resonant interactions; $J_{n,m}$ is the resonant Coulomb coupling between molecules m and n ; The ket $|n\rangle$ represents a local excited state where the n th chromophore is electronically excited to the excited state while all other molecules remain in their electronic ground state. When periodic boundary conditions are imposed, the eigenstates of H_{ex} are the wavelike excitations of excitons characterized by a dimensionless wave vector (k). The energy of the k th exciton (E_k) is given by

$$E_k = E_M + D + J_k \quad (\text{S19})$$

where J_k is the k -dependent component of the Coulombic coupling. When only the nearest neighbor (n.n.) coupling is retained, one obtains

$$J_k = 2\Delta\varepsilon \cos(k) \quad (\text{S20})$$

5. Time-dependent density functional theory (TD-DFT) calculation

All theoretical calculation was carried out at the B3LYP/6-31G(d) level using density functional theory (DFT) in the Gaussian 09 software⁸. The excitation energies in the n -th singlet (S_n) and n -th triplet (T_n) states were obtained using the TD-DFT method based on an optimized molecular structure at ground state (S_0). The π - π stacked H-aggregated states of the dimers were calculated with B3LYP/6-31G(d) to take into consideration the weak long-range intermolecular interactions. The triplet energy stabilization energy was calculated by the difference between the total molecular energy of the dimer and a sum of the total molecular energy of the two monomers on S_0 and the lowest triplet excited state (T_1), respectively. Spin-orbit coupling (SOC) matrix elements between the singlet and triplet excited states are calculated with quadratic response function methods using the Dalton program. The SOCs of molecules presented in **Table S4** were performed at the optimized geometry at T_1 state using B3LYP functional and cc-pVDZ basis set⁹, while the SOCs of *m*CNPhCz and *m*CNPhCz' presented in **Figure 2** were performed on the crystal structure with the same method but without the structure optimization.

Table S4. TD-DFT-calculated energy levels at singlet (S_1) and triplet (T_n) states and spin-orbit coupling (SOC) results between S_1 and T_n of **PhCz**, **pCNPhCz**, **mCNPhCz**, **oCNPhCz** and **DCNPhCz**; the most possible ISC channel was marked in red.

Compounds	$S_1 \rightarrow T_n$	S_1 (eV)	T_n (eV)	ΔE_{ST} (eV)	SOC (cm^{-1})
PhCz	$S_1 \rightarrow T_1$	3.73	2.47	1.26	0.10
	$S_1 \rightarrow T_2$	3.73	3.08	0.65	0.07
	$S_1 \rightarrow T_3$	3.73	3.53	0.2	0.36
	$S_1 \rightarrow T_4$	3.73	4.01	-0.28	0.31
	$S_1 \rightarrow T_5$	3.73	4.06	-0.33	0.55
	$S_1 \rightarrow T_6$	3.73	4.08	-0.35	0.22
pCNPhCz	$S_1 \rightarrow T_1$	3.52	2.97	0.55	0.11
	$S_1 \rightarrow T_2$	3.52	3.17	0.35	8.47
	$S_1 \rightarrow T_3$	3.52	3.43	0.09	7.14
	$S_1 \rightarrow T_4$	3.52	3.77	-0.25	3.24
	$S_1 \rightarrow T_5$	3.52	3.79	-0.27	5.90
	$S_1 \rightarrow T_6$	3.52	3.87	-0.36	1.49
mCNPhCz	$S_1 \rightarrow T_1$	3.40	3.09	0.31	0.40
	$S_1 \rightarrow T_2$	3.40	3.17	0.22	7.68
	$S_1 \rightarrow T_3$	3.40	3.41	-0.01	13.86
	$S_1 \rightarrow T_4$	3.40	3.44	-0.05	17.86
oCNPhCz	$S_1 \rightarrow T_1$	3.25	3.05	0.20	2.08
	$S_1 \rightarrow T_2$	3.25	3.18	0.08	10.88
	$S_1 \rightarrow T_3$	3.25	3.44	-0.19	8.43
	$S_1 \rightarrow T_4$	3.25	3.45	-0.20	28.65
	$S_1 \rightarrow T_5$	3.25	3.58	-0.33	10.20
DCNPhCz	$S_1 \rightarrow T_1$	2.97	2.78	0.19	0.45
	$S_1 \rightarrow T_2$	2.97	2.95	0.01	7.89
	$S_1 \rightarrow T_3$	2.97	3.16	-0.20	7.39
	$S_1 \rightarrow T_4$	2.97	3.31	-0.34	5.38

Table S5. Aggregation structures of *p*CNPhCz, *m*CNPhCz, *m*CNPhCz', *o*CNPhCz and DCNPhCz crystals investigated by Frenkel exciton theory through the nearest neighboring dimers. When the splitting energy ($\Delta\epsilon$) > 0, this pair of dimer belongs to H-aggregation (in red), and when $\Delta\epsilon$ < 0, it is J-aggregation (in black).

Compounds	Dimer	α (°)	ϑ_1 (°)	ϑ_2 (°)	M (Debye)	r (Å)	E_{S1} (eV)	E_{T1} (eV)	$\Delta\epsilon$ (eV)
<i>p</i> CNPhCz	4 0	0.0	95.6	95.6	4.25	10.28	3.73	3.15	0.0202
	4 8	0.0	84.4	84.4	4.25	10.28	3.73	3.15	0.0202
	4 10	180.0	35.5	144.5	4.25	9.44	3.50	3.02	0.0265
	4 11	180.0	14.0	166.0	4.25	14.15	3.76	3.18	0.0145
	4 17	180.0	28.8	151.2	4.25	9.91	3.73	3.18	0.0302
	4 45	67.5	95.9	59.3	4.25	9.93	3.72	3.15	0.0124
	4 48	67.5	150.6	89.8	4.25	6.96	3.71	3.14	0.0261
	4 49	67.5	90.2	29.4	4.25	6.96	3.71	3.14	0.0261
	4 52	67.5	120.7	84.1	4.25	9.93	3.72	3.15	0.0124
	4 1	0.0	52.5	52.5	4.25	8.27	3.70	3.14	-0.0045
	4 3	0.0	134.7	134.7	4.25	8.59	3.74	3.16	-0.0172
	4 5	0.0	45.3	45.3	4.25	8.59	3.74	3.16	-0.0172
	4 7	0.0	127.5	127.5	4.25	8.27	3.70	3.14	-0.0045
	4 16	180.0	57.1	122.9	4.25	4.87	3.52	3.03	-0.0227
<i>m</i> CNPhCz	28 2	40.8	87.9	88.4	1.42	8.67	3.38	3.03	0.0029
	28 3	40.8	89.3	95.9	1.42	8.67	3.38	3.03	0.0030
	28 4	40.8	94.8	78.1	1.42	9.20	3.42	3.12	0.0026
	28 5	40.8	96.1	85.2	1.42	9.20	3.43	3.12	0.0025
	28 9	170.6	156.1	30.6	1.42	9.51	3.55	3.14	0.0041
	28 11	170.6	169.8	11.9	1.42	10.00	3.56	3.15	0.0048
	28 18	170.6	33.4	144.7	1.42	12.71	3.53	3.13	0.0013
	28 20	170.6	44.0	138.2	1.42	12.46	3.58	3.16	0.0008
	28 25	130.6	134.6	45.4	1.42	11.31	3.53	3.13	0.0015
	28 27	0.0	74.1	74.1	1.42	3.96	3.42	3.08	0.0316
	28 29	0.0	105.9	105.9	1.42	3.96	3.42	3.08	0.0316
	28 31	148.2	8.6	151.9	1.42	10.17	3.42	3.07	0.0043
28 32	130.6	37.5	163.1	1.42	10.17	3.42	3.07	0.0039	
<i>m</i> CNPhCz'	28 3	170.9	45.0	136.8	1.16	12.35	3.47	3.16	0.0005
	28 4	170.9	139.2	35.7	1.16	8.95	3.41	3.12	0.0020
	28 5	170.9	145.3	43.1	1.16	8.54	3.39	3.11	0.0022
	28 16	45.4	77.6	105.9	1.16	4.79	3.27	3.02	0.0134
	28 17	45.4	80.7	93.4	1.16	4.79	3.27	3.02	0.0112
	28 1	170.9	75.1	111.6	1.16	8.97	3.44	3.14	-0.0016
	28 13	45.4	29.1	36.7	1.16	11.56	3.37	3.09	-0.0015
	28 20	45.4	135.8	160.0	1.16	11.56	3.37	3.09	-0.0014
	28 24	0.0	24.3	24.3	1.16	10.23	3.45	3.14	-0.0023
	28 32	0.0	155.7	155.7	1.16	10.23	3.45	3.14	-0.0023
	28 36	132.6	80.8	146.5	1.16	9.55	3.37	3.09	-0.0005
	28 38	132.6	33.5	99.2	1.16	9.55	3.37	3.09	-0.0005
28 40	132.6	145.5	81.8	1.16	9.47	3.29	3.06	-0.0006	

	28 42	132.6	98.2	34.5	1.16	9.47	3.29	3.06	-0.0006
oCNPhCz	33 14	101.6	29.9	123.5	1.48	9.99	3.23	3.08	0.0034
	33 18	59.9	51.4	102.9	1.48	7.80	3.23	3.08	0.0053
	33 20	102.4	114.2	30.6	1.48	6.90	3.29	3.13	0.0070
	33 21	0.8	67.7	66.9	1.48	8.05	3.18	3.15	0.0029
	33 26	101.6	56.5	150.1	1.48	9.99	3.23	3.08	0.0034
	33 29	134.0	23.2	156.8	1.48	11.32	3.30	3.13	0.0035
	33 30	59.9	76.6	129.1	1.48	7.80	3.23	3.08	0.0054
	33 32	101.0	148.7	67.6	1.48	6.90	3.29	3.13	0.0066
	33 45	0.1	112.3	112.4	1.48	8.05	3.18	3.15	0.0030
	33 22	134.1	89.2	64.7	1.48	7.14	3.18	3.04	-0.0054
	33 31	59.6	156.6	108.3	1.48	9.28	3.28	3.12	-0.0012
	33 34	133.3	114.5	91.7	1.48	7.14	3.18	3.04	-0.0054
	33 35	134.4	96.8	83.4	1.48	8.72	3.33	3.15	-0.0027
DCNPhCz	6 2	0.0	58.0	58.0	0.63	4.73	3.09	2.89	0.0008
	6 5	116.1	52.6	110.0	0.63	9.41	3.01	2.80	0.0001
	6 9	116.1	70.0	127.4	0.63	9.41	3.01	2.79	0.0001
	6 10	0.0	122.0	122.0	0.63	4.73	3.09	2.89	0.0008
	6 18	160.8	124.9	54.4	0.63	12.73	3.14	2.92	0.0001
	6 19	160.8	126.9	49.4	0.63	14.26	3.16	2.92	0.0001
	6 20	160.8	128.0	45.8	0.63	16.02	3.16	2.93	0.0001
	6 3	116.1	83.2	80.2	0.63	8.68	3.12	2.90	-0.0004
	6 4	82.6	36.1	51.5	0.63	9.59	3.15	2.92	-0.0008
	6 7	116.1	99.8	96.8	0.63	8.68	3.12	2.90	-0.0004
	6 13	160.8	110.1	84.3	0.63	13.24	3.15	2.92	-0.0002
	6 15	160.8	127.6	64.6	0.63	11.56	3.15	2.93	-0.0001
	6 16	82.6	147.4	124.9	0.63	9.59	3.15	2.92	-0.0007

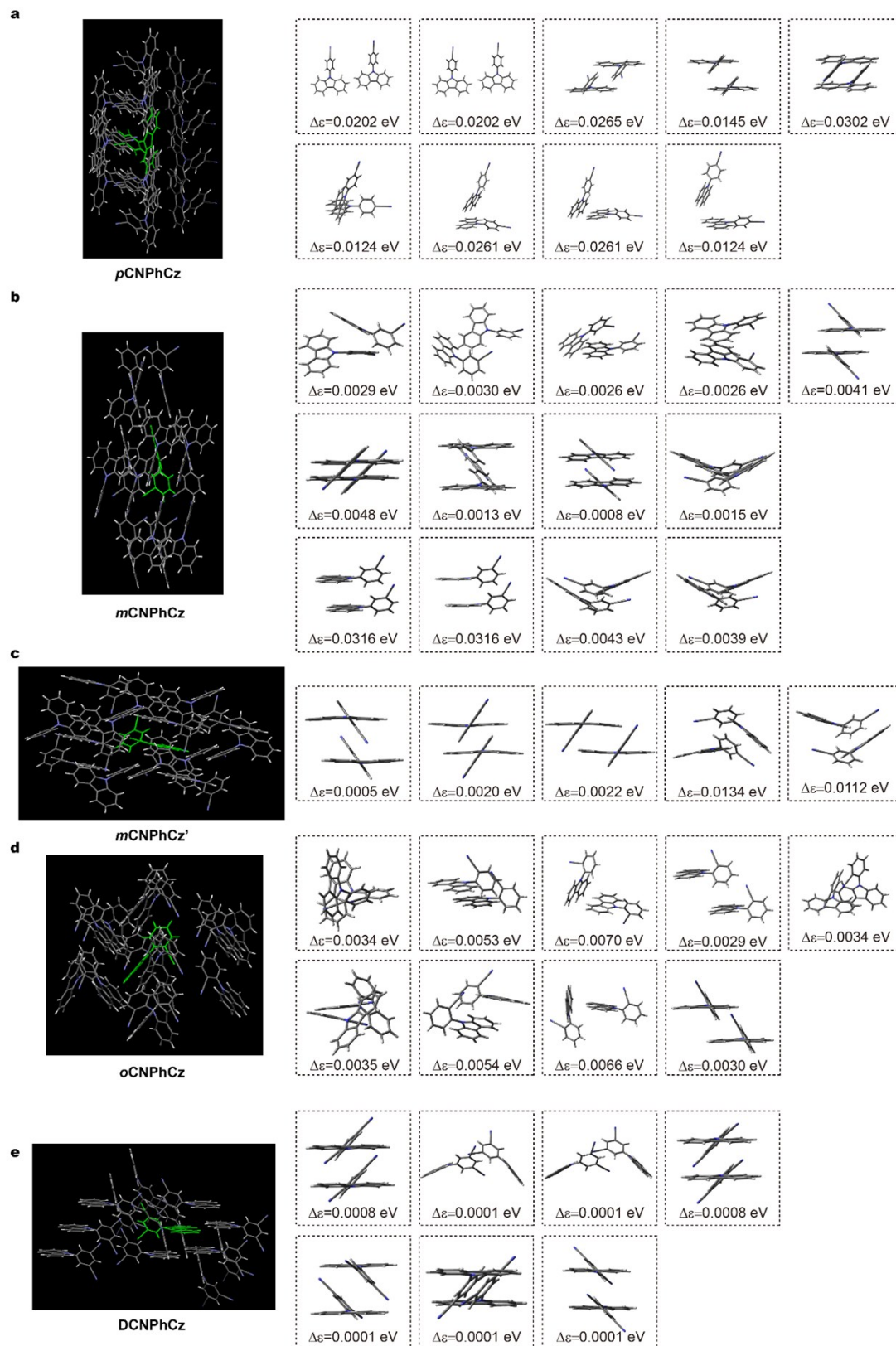


Figure S15. Aggregation structures of (a) **pCNPhCz**, (b) **mCNPhCz**, (c) **oCNPhCz** and (d) **DCNPhCz** crystals.

6. Bioimaging application

With a top-down method, water-dispersible **DCNPhCz** nanoparticles were prepared by encapsulating an amphiphilic triblock copolymer of Poly(ethyleneglycol)-block-poly(propyleneglycol)-block-poly(ethyleneglycol) (PEG-*b*-PPG-*b*-PEG) (F127, molecular weight = 12.6 kDa)^{10,11}. The encapsulation of **DCNPhCz** crystal was performed on an ultrasonic cell disruptor (SONICS & MATERIALS INC., VCX 130). The size distribution of the **DCNPhCz** nanoparticles was measured on a Brookhaven ZetaPALS. Transmission electron microscopy (TEM) was taken on a JEOL JEM-2100 transmission electron microscope at an acceleration voltage of 150 kV.

Nanoparticle preparation: **DCNPhCz** powder (3 mg) in microcrystals was added to an aqueous solution of F127 (6.0 mg/mL, 1.0 mL) under continuous sonication with a microtip-equipped probe sonicator for 10 min. Then, the aqueous solution was filtered through a 0.22 μm polyvinylidene fluoride (PVDF) syringe-driven filter (Millipore) to get the **DCNPhCz** nanoparticles.

Bioimaging: For the cellular imaging, the above prepared **DCNPhCz** nanoparticles was diluted 1000 times and incubated with living HeLa cells (breast cancer cells) for 2 h at 37°C. Confocal images were taken by a confocal microscopy (Olympus FV1000MPE). Molecular bio-imaging was acquired by the confocal microscopy in a cell incubator at 37°C with temperature control resolution $\pm 0.1^\circ\text{C}$ under the excitation of a 405 nm diode laser.

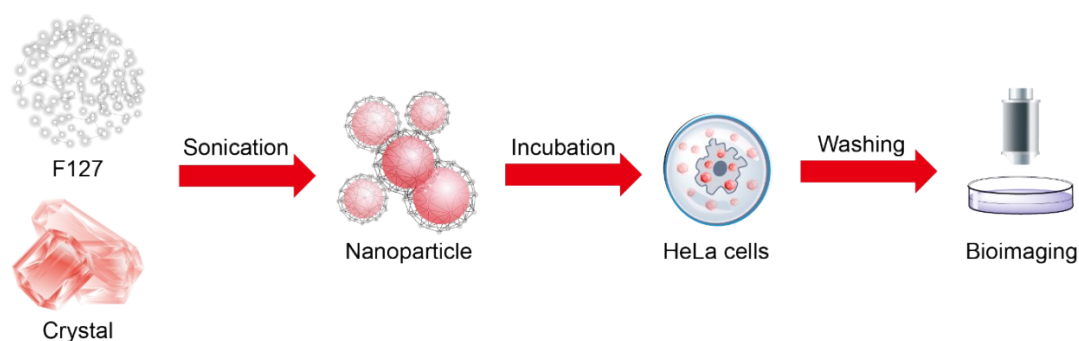


Figure S16. Top-down preparation of **DCNPhCz** nanoparticles for molecular bio-imaging of HeLa cells.

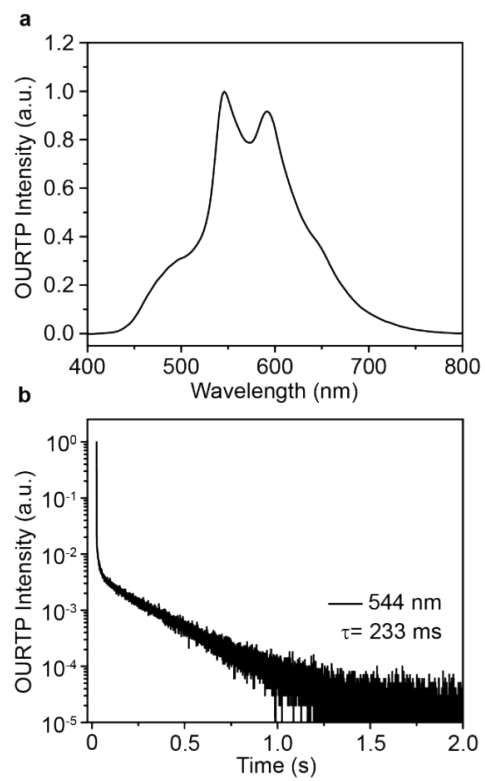


Figure S17. OURTP spectrum (a) and lifetime decay profile (b) of **DCNPhCz** nanoparticles dispersed in deionized water under the excitation wavelength of 400 nm at room temperature. A delay time of 10 ms was applied to measure the OURTP spectrum.

References:

1. J. Hassan, M. Seignon, C. Gozzi, E. Schulz, M. Lemaire, *Chem. Rev.*, 2002, **102**, 1359.
2. C. Y. Joo, Y. K. Soo, L. J. Yeob, *Adv. Mater.*, 2014, **26**, 4050.
3. Z. Sun, J. Luo, J. Zhang, C. Ji, L. Zhou, S. Li, F. Deng, M. Hong, *Adv. Mater.*, 2013, **25**, 4159.
4. S. Saha., A. Samanta., *Acta Crystallogr., Sect. C*, 1999, **55**, 1299.
5. Z. An, C. Zheng, Y. Tao, R. Chen, H. Shi, T. Chen, Z. Wang, H. Li, R. Deng, X. Liu, W. Huang, *Nature Materials*, 2015, **14**, 685.
6. S. Lower, M. El-Sayed, *Chem. Rev.*, 1966, **66**, 199; D. R. Scott, O. Maltenieks, *J. Phys. Chem.*, 1968, **72**, 3354.
7. J. Birks, *Rep. Prog. Phys.*, 1975, **38**, 903.
8. M. R. Frisch, G. W. Trucks , H. B. Schlegel , G. E. Scuseria, M.A. Robb, Gaussian 09 Gaussian. Inc.: Wallingford, CT, 2009.
9. Q. Peng, Q. Shi, Y. Niu, Y. Yi, S. Sun, W. Li, Z. Shuai, *J. Mater. Chem. C*, 2016, **4**, 6829
10. X. Zhen, Y. Tao, Z. An, P. Chen. C. Xu, R. Chen, W. Huang, K. Pu, *Adv. Mater.*, 2017, **29**, 1606665.
11. J. Yang, X. Zhen, B. Wang, X. Gao, Z. Ren, J. Wang, Y. Xie, J. Li, Q. Peng, K. Pu, Z. Li, *Nature Commun.*, 2018, **9**, 840.